The Aging Response of a Welded Iron-Based Superalloy

An alloy with improved hot cracking resistance exhibits pronounced differences in aging response and resulting strength level between base and weld metal regions

BY M. J. STRUM, L. T. SUMMERS AND J. W. MORRIS, JR.

ABSTRACT. GTA weldments of JBK-75, a superalloy with improved hot cracking resistance, exhibit pronounced differences in aging response and resultant strength level between base and weld metal regions. The iron-based superalloys are primarily age-hardened materials strengthened through precipitation of a fine dispersion of gamma prime, Ni_3Ti, in an austenite matrix. The presence of titanium segregation to dendrite interstices upon weld metal solidification results in a nonuniform aging response within the weld.

Although rapid initial precipitation occurs within the weld, a persistent mismatch between the base metal and the lower hardness weld metal is suffered irrespective of aging time. This behavior is explained by the localization of slip occurring within the weld solidification structure. Uniform hardness levels can be obtained with short time, moderate temperature, post weld anneals at 950°C (1742°F) prior to aging.

Introduction

This paper describes the effect of welding on the aging response and structure-property relationships in the iron-based superalloy designated as JBK-75. This investigation was prompted by tensile test observations of a persistent strength mismatch between base metal and weaker weld metal regions. Knowledge of the base metal aging response alone is therefore no longer sufficient to optimize weldment mechanical performance.

M. J. STRUM, L. T. SUMMERS and J. W. MORRIS, JR. are associated with the Department of Materials Science and Mineral Engineering, and Materials and Molecular Research Division, Lawrence Berkeley Laboratory, University of California, Berkeley, California.

JBK-75 is an iron-based superalloy precipitation hardened by a fine dispersion of gamma-prime, $Ni_3(Ti,Al)$, in an austenite matrix. The alloy is similar to A-286 (Table 1), but modified to increase high temperature strength and ductility leading to improved hot cracking resistance (Refs. 1, 2).

Strength mismatch can have large consequences in applications where the weld metal is subjected to stress levels similar to those in the rest of the weldment. The stress applied to the structure is now limited by the strength of the weaker weld. Additionally, although the weld may be very ductile, accommodational strains will be concentrated in the weaker weld region resulting in failure after relatively small total strains. Total strain before failure will continually decrease with increasing effective gage lengths, which include the weld region. Of course, the magnitude of these problems will also depend on the degree of strength mismatch present.

In an attempt to discover the origin of the strength mismatch, weld metal and base metal aging responses were studied.

Table 1—Chemical Analysis Results, Wt-%

	JBK-75		
	Heat 1	Heat 2	A-286
Fe	Bal.	Bal.	Bal.
Cr	15.5	14.4	14.5
Ni	29.8	28.5	25.4
Ti	2.05	2.15	2.25
Al	0.24	0.20	0.22
Mo	1.25	1.20	1.30
V	0.27	0.27	0.26
Mn	0.05	—	1.50
Si	.018	—	0.58
C	.016	.016	.063
P	.002	.005	.004
S	18 ppm	.006	.005
B	< 5 ppm	.0018	.0073

Differences in aging response are very important to the strength levels attained in this primarily precipitation-hardened alloy. Electrical resistance measurements during isothermal aging at 725°C (1337°F) were used to obtain information on early stage precipitation. Hardness curves of base metal and weld metal regions were used to determine the effect of aging time and treatment on strength.

Two major factors seem to influence the decreased hardness level in the weld. The first is the dendritic solidification structure. Segregation of titanium, the major hardening element in JBK-75, to the dendrite interstices was verified using auger electron spectroscopy. The effect of titanium segregation on the weld metal aging response was examined by hardness measurements and deformation induced slip-step observations. These tests were performed both before and after postweld annealing treatments at 950°C (1742°F). The effect of postweld treatments on homogenization of the weld was evidenced by the reduction in localized deformation within the weld solidification structure.

The second factor contributing to the mismatch is the larger columnar grains in the weld metal relative to the fine equiaxed base metal microstructure. Microhardness traverses across the weld zones displayed the effect of increased grain size in both the weld and heat-affected zones. Recrystallized weld metal grains, achieved through a post-weld thermomechanical treatment, further indicated the magnitude of the grain size effect on the mismatch by matching base metal and weld metal grain sizes for hardness comparison. Significant reductions in the as-solidified weld metal grain size is difficult in a fully austenitic steel, and beyond the scope of this work. However, some success has been achieved by others using mechanical

Table 2—JBK Tensile Properties[a]

Conditions		Yield strength,		Tensile strength,		% Elongation(s) in			
Temperature, K[b]	Speciman type	MPa	(ksi)	MPa	(ksi)	25.4 mm (1 in.)	12.7 mm (½ in.)	6.3 mm (¼ in.)	Reduction in area, %
298	Base	965	(140)	1215	(176)	17	21		41
	Weld	841	(122)	945	(137)	4	7.5	16	26
77	Base	1105	(160)	1530	(222)	23	25		27
	Weld	972	(141)	1215	(176)	6	10	19	32
4.2	Base	1180	(171)	1600	(232)	16	14		33
	Weld	1130	(164)	1385	(201)	6.5	11	21	32

(a) Standard heat treatment: 725°C (1337°F) for 24 h + 650°C (1202°F) for 24 h.
(b) 298 K = 25°C (77°F); 77 K = −196°C (−321°F); 4.2 K = −269°C (−452°F).

vibrations, arc or torch modulation, magnetic stirring, and carbide impregnation (Ref. 3-6).

Tensile Mismatch

In evaluating candidate materials for the force-cooled superconducting coil jacket (Ref. 7), tensile tests were performed on base material and weldments of JBK-75. All welds in this study were autogenous (without filler metal) and were made in butted plates using the gas tungsten arc process (GTA). Plate thickness was approximately 3.2 mm (0.125 in.). For maximum uniformity of mechanical properties through the weld zones after aging, all welding was performed on material in the solution-annealed condition. The solution annealing treatment of 1 hour (h) at 900°C (1652°F) following 75% reduction by cold rolling resulted in a grain size of between ASTM 9 and 10.

Tensile tests were performed using ASTM standard flat tensile specimens with 25.4 mm (1 in.) gage lengths. Weldment specimens were cut such that the approximately 3 mm (⅛ in.) wide weld metal region was centered on the gage length with the tensile direction transverse to the weld length and ground flat. Therefore, weld metal, HAZ and base metal regions were all included in the gage lengths of the welded test specimens. Gage marks were scratched onto the specimens and measured both before and after testing using a travelling microscope with an accuracy of ±0.01 mm (±0.0004 in.). Gage lengths of 6.35, 12.7 and 25.4 mm (¼, ½ and 1 in.) were used on welded specimens to indicate the relative ductility of the weld metal in the composite specimen. Total elongations were thus measured directly. Reduction in area data were estimated from measurements of maximum reductions in gage widths. The yield strengths reported were found using 0.2% offset strain levels. Cryogenic testing at 77 and 4.2 K (−196 and −452°F) was accomplished by complete immersion of the tensile specimen in liquid nitrogen or liquid helium during testing using a compression tube and appropriate cryostat.

As can be seen in Table 2 and Fig. 1, a persistent strength mismatch exists between base metal and weldment specimens. Although all fracture surfaces indicate ductile rupture, weldment specimens consistently failed in the lower strength weld metal. This resulted in low total elongations over the 25.4 mm (1 in.) gage even though the weld metal was very ductile as evidenced by the reduced gage length elongation data. The lower strength weld metal thus causes strain localization in the weldment specimen. The magnitude of this strength mismatch was observed to decrease with test temperature. This may be rationalized by an increased resistance to the slip localization within the weld solidification structure, discussed later, due to increased resistance to the cross-slip of screw dislocations at cryogenic temperatures.

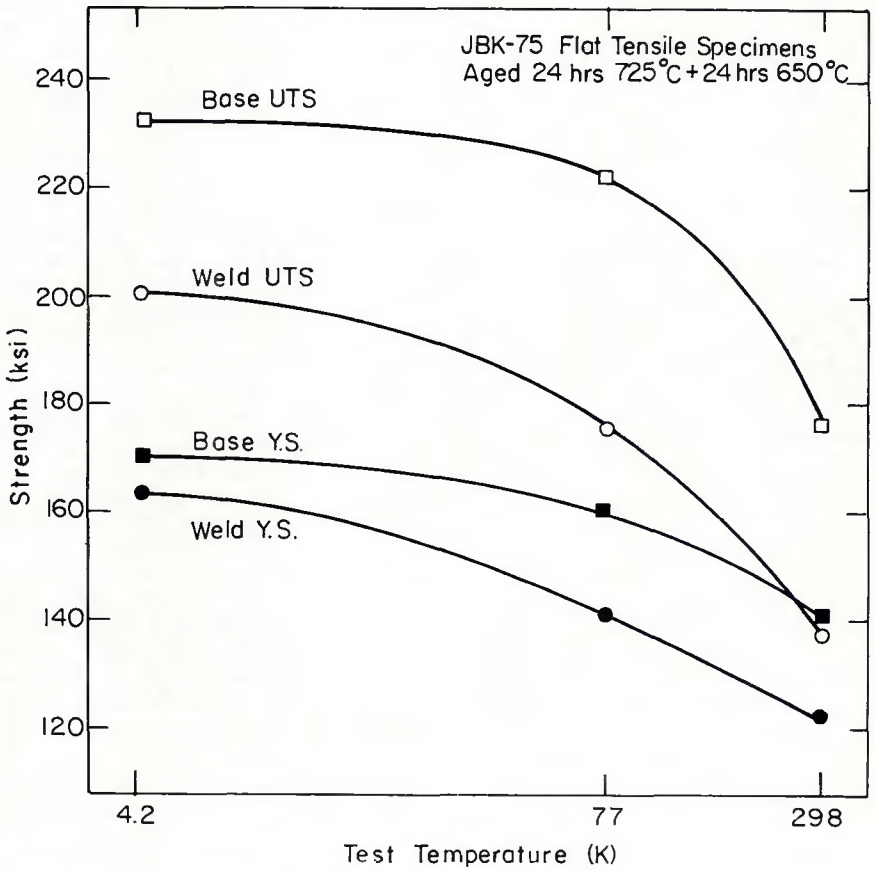

Fig. 1—JBK-75 tensile strength vs. temperature

Electrical Resistance Curves

Electrical resistance curves were prepared as plots of resistivity changes occurring during isothermal aging at 725°C (1337°F). The resistance increases were mainly due to the formation of Guinier-Preston zones, the earliest stage of precipitation. It is believed (Ref. 8-10) that the resistivity maximum is associated with a critical zone diameter of about 10Å causing maximum scattering of the conduction electrons. The maximum resistance increase should then be proportional to the density of zones of approximately critical diameter. Both

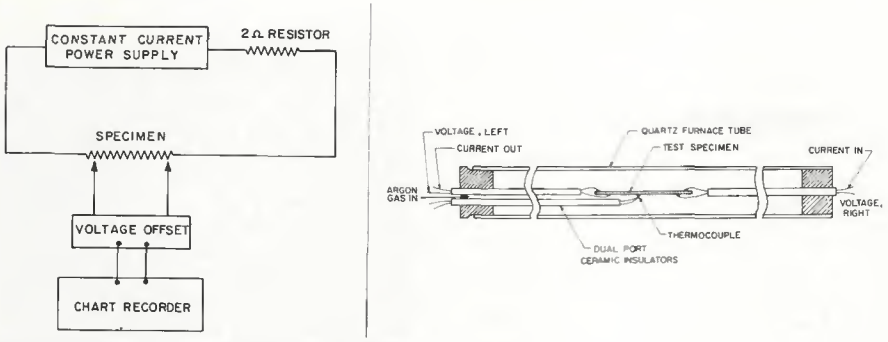

Fig. 2—Electrical resistance test configuration

smaller and larger zone diameters should result in decreased resistivities.

The experimental configuration is shown in Fig. 2. Using a constant current power source, any resistance changes resulted in a change of potential across the sample. Using current levels of approximately 1 ampere (A), the potential drops across 50 mm (1.97 in.) of the 75 mm (2.95 in.) long samples were about 30 millivolts. Using a voltage offset (suppression) device, the sensitivity of the recorder was set to one millivolt full scale deflection. Both current and voltage leads of Fe-Cr-Al-Co furnace element wire were spot welded onto the strip samples. A thermocouple was also spot welded to the center of the sample for temperature records. Aging treatments were performed at 725°C (1337°F) in a tube furnace in argon. The data plotted are the percentage changes from the initial resistivity as a function of aging time. Two tests of each the base metal and weld metal samples were performed. The data presented are the average of the two experimental curves obtained for each sample type.

Comparison of the base metal and weld metal resistance curves in Fig. 3 evidence a faster aging response in the weld metal. The time to peak resistance is only about 20 minutes (min) in the weld metal vs. 50 min in the base metal samples. But the weld metal samples also exhibit a lower peak resistance increase and a more rapid decrease relative to base metal samples. Although the resistance method is very sensitive to early stage precipitation, no evidence of latter stage equilibrium precipitation was seen. Interpretation of observed differences between the two curves is discussed later, using weld metal segregation arguments.

Hardness Curves

Hardness testing was performed on both base metal and weld metal regions. After welding and heat treating, the specimens were ground until both top and bottom surfaces were flat and parallel using a surface grinder with an aluminum oxide wheel. Specimens were then polished through a series of SiC wet papers of grit sizes 240 to 600. Resulting specimen thicknesses were approximately 2 mm (0.08 in.). Last, the specimens were macro-etched in Keller's concentrated etch of mixed acid in distilled water. This allowed centering of the indentor during hardness tests on the weld centerline, improving the accuracy and consistency of weld metal hardness data.

A Wilson Rockwell hardness tester was used for the hardness measurements. For samples harder than R_c 20, "C" scale tests were used with a 150 kg (330.7 lb) major load and diamond brale indentor. An escape time of 20 seconds(s) was set as standard. Softer samples were tested on the "B" scale with a 100 kg (220 lb) major load and a 1.6 mm (0.06 in.) steel ball indentor. Using a Wilson conversion chart these values were converted into equivalent "A" scale values for data presentation. At least six indentions were made and the readings averaged for each data point. The error bars in the hardness curves are average values plus or minus the standard deviation in the readings.

Hardness-aging curves provide resultant strength level indications as the precipitation sequence progresses during isothermal aging. Both base metal and weld centerline hardness curves are plotted in Fig. 4 and 5. These display the weldment aging responses at 725°C (1337°F) in the as-welded condition and at 725°C (1337°F) after 25% postweld cold reduction respectively. In each case the weld metal exhibits a slower age-hardening response, lower peak hardness and persistent strength mismatch with the base metal. It can also be seen that the weld metal continues to harden long after the base metal has reached its peak level and begun to soften or overage.

Although the weld metal hardness approaches that of the base metal after very long aging times at 725°C (1337°F), this is not a practical heat treatment. Both base metal and weld metal possess significant amounts of a cellular grain boundary phase believed to be the equilibrium eta phase, Ni_3Ti, after 125 h at 725°C (1337°F). This phase heterogeneously nucleates and grows from the columnar grain boundaries in the weld, as seen in Fig. 6. The large misfit between the HCP equilibrium eta phase and the FCC matrix favors precipitation of the metastable ordered FCC gamma-prime precipitates at low aging temperatures and short aging times (Refs. 11-13). However, no indication of the precipitation of the cellular phase appears on the hardness curves. Thus, it appears that the hardness behavior after long aging times is governed more by the overgrowth of gamma-prime precipitates to sizes allowing

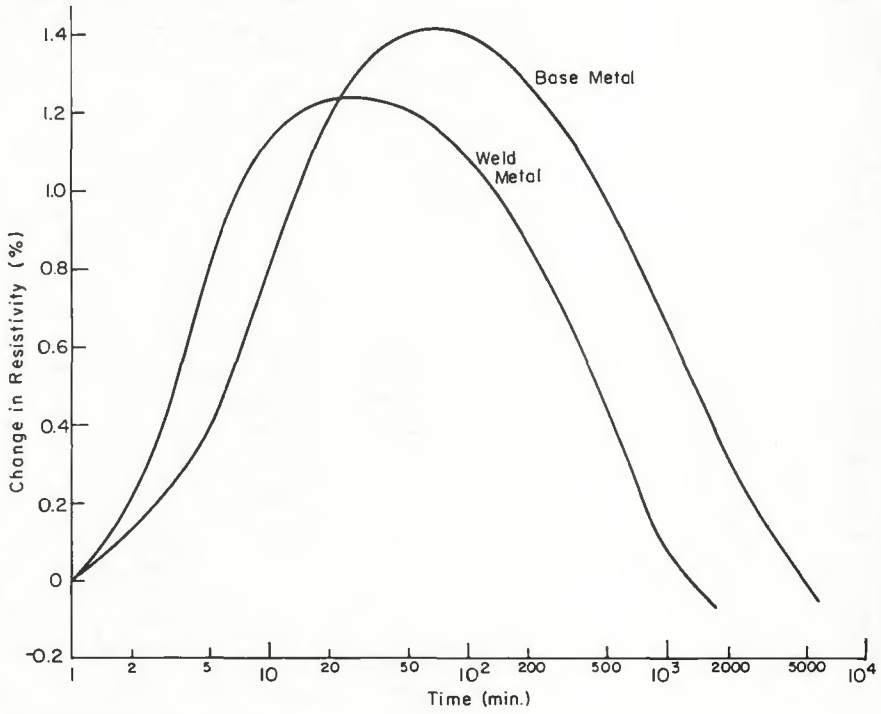

Fig. 3—Electrical resistance curves

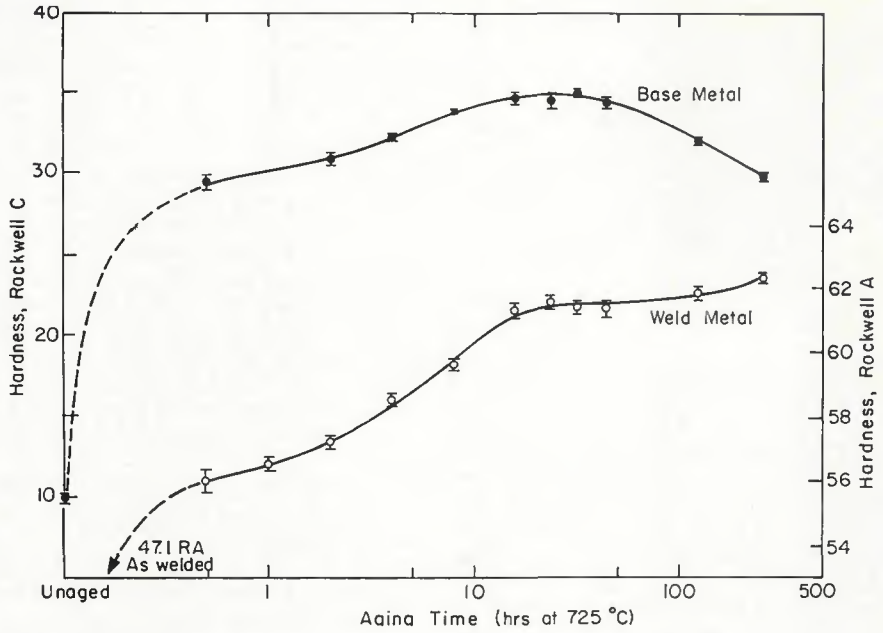

Fig. 4—Hardness curve at 725°C (1337°F)

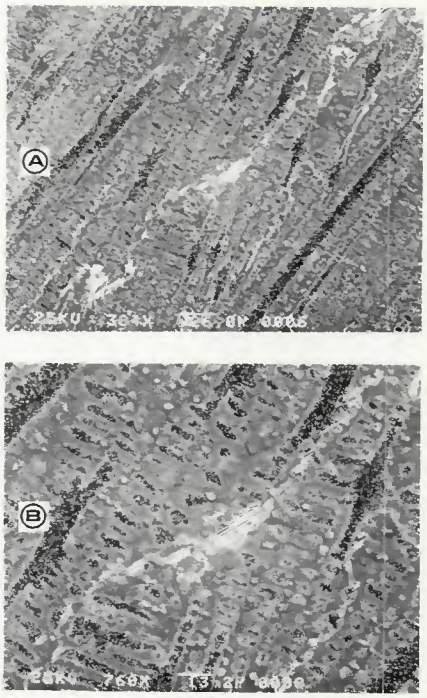

Fig. 6—Overaged etched microstructure: A—X384; B—X760 (A and B reduced 50% on reproduction)

dislocation by-passing than by the presence of the cellular phase. However, presence of the cellular phase, forming brittle grain boundary layers must usually be avoided.

From early tensile results of weldments given 10% cold work prior to aging, it appeared that such treatments may be beneficial in reducing weldment anisotropy. But even after 25% uniform cold work prior to aging, the large mismatch persists. However, the aging response is greatly accelerated, with peak base metal hardness occurring after only 1 h. Weld hardness continues to increase as base metal softens but reaches a plateau after only 4 h at 725°C (1337°F). The peak hardness levels are much improved with the weld hardness peak approaching the base metal hardness peak level in the as-welded and aged condition.

Segregation

The apparent disparity of aging behavior as evidenced by electrical resistance measurements and hardness curves can be explained through the existence of dendritic segregation. Segregation during weld solidification is usually identified with hot cracking problems. Typically, solute rejection at the advancing solid/liquid interface results in the formation of low melting-point eutectics or solute-rich regions at the dendrite interstices (Refs. 1, 14-17). Shrinkage strains cause the initiation and propagation of cracks through these degraded regions still near their melting points.

A-286 is an alloy well known for its high susceptibility to weld hot cracking when welded under conditions of high restraint as in thick sections. This susceptibility was drastically reduced in JBK-75 by modification of the equilibrium and properties of the segregated low melting phase through removal of Si and Mn additions and lowering B and C while increasing Ni levels (Refs. 1, 2). However, although cracking problems were not encountered in this investigation, segregation of titanium, the major hardening element, to interdendritic regions on solidification is shown to alter the subsequent aging response and strength levels in the weld.

The presence of segregation in JBK-75 welds is evidenced by severe coring upon etching. This allows observation of the solidification structure due to the preferential attack of dendritic regions with a mixed-acid etching solution. Solute rejection of titanium to the interdendritic regions is evidenced by the presence of small titanium-rich precipitates exclusively at the dendrite interstices in as-welded specimens. These precipitates include both the titanium and titanium-molybdenum carbides also found randomly dispersed in the base metal and a highly substituted phase believed to be the $(Fe,Ni,Cr)_{24}(Ti,Mo)_5$ topologically close-packed χ phase often found in A-286 (Refs. 12, 18, 19) but not reported in a thorough study of JBK-75 base metal precipitation (Ref. 23). These precipitates were identified from Kevex quantitative chemical analysis in the scanning electron microscope.

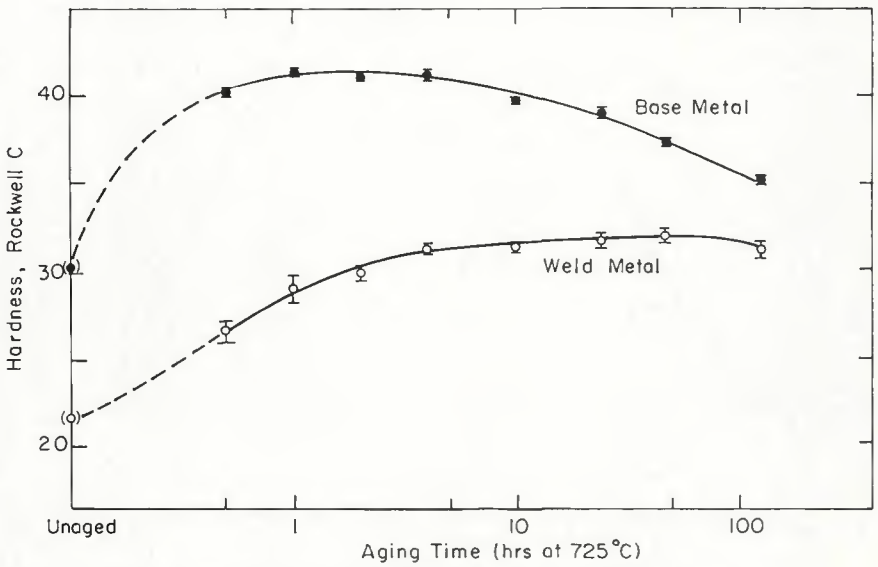

Fig. 5—Hardness curve at 725°C (1337°F) after 25% cold work before aging

The magnitude of titanium segregation has been documented by auger electron spectroscopy. Line scans across the solidification structure give the concentration profile of titanium in Fig. 7. The nominal 2.5 at-% titanium concentration is seen to fluctuate between a minimum of 1.0 at-% at dendrite cores to maxima of about 5 at-% at interdendritic regions, with a 1 μm beam size. Spot analyses along the line scan revealed no indication of Ni, Cr, or Fe segregation.

These large variations in titanium concentration within the solidification structure result in a non-uniform aging response in the weld metal. The titanium-enriched regions are expected to display both rapid initial precipitation of γ' and a higher density of nuclei due to increased supersaturation. Titanium depleted regions are expected to possess fewer nuclei with corresponding large average precipitate sizes. These phenomena were observed by Clark and Pickering (Ref. 20) using transmission electron microscopy in 15Cr, 25Ni, iron-based alloys with titanium contents between 2.0 and 3.85 wt-%.

Similarly, Owzcarski and Sullivan (Ref. 21) have reported observations of large γ' particles formed near the solvus temperature in a welded nickel-based superalloy that delineate the regions of coring of the original, as-cast structure. The resistance curve data can thus be interpreted as consistent with the expected aging response. The rapid initial resistance increase in the weld metal specimen can be associated with rapid precipitation in titanium-enriched regions. The lower peak resistance increase and more rapid decrease are consistent with a low density of precipitates and early coarsening above the 10Å critical precipitate diameter in the titanium depleted regions.

Evidence of large variations in precipitate size and density in JBK-75 welds can be seen in the SEM observations of the overaged microstructure. After 250 h at 725°C (1337°F), as shown in Fig. 6, there is a marked difference in contrast between the dendritic regions (darker areas in Fig. 6) and interdendritic regions (lighter toned areas). Although resolution of individual precipitates cannot be observed in the dendritic regions, large precipitates surrounded by precipitate-free areas are easily observed at interdendritic areas. Thus, it appears that titanium-depleted regions corresponding to the dendrite cores result in limited nucleation events and early precipitate coarsening. This is consistent with the expected changes in the precipitation kinetics as the degree of supersaturation at the aging temperature decreases with titanium depletion.

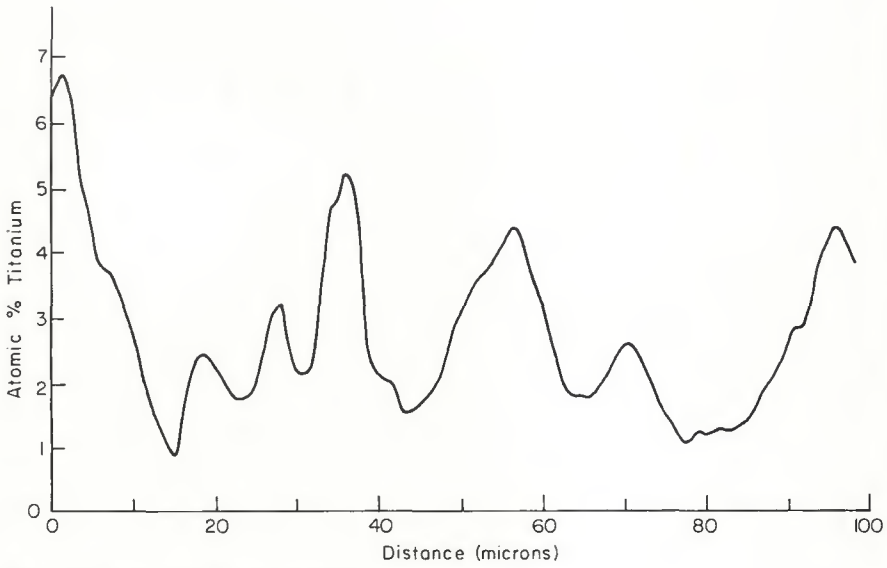

Fig. 7 – Titanium concentration profile

The segregation of titanium resulting in non-uniform precipitation behavior also affects the hardness levels in the weld metal. In an aging study of a series of Fe–15% Cr–20% Ni–Ti steels with titanium contents of 1.5 to 3.75% by Blower and Mayer (Ref. 22), hardness levels were seen to increase steadily with increasing titanium content after any identical aging treatment up to 100 h at either 700 or 750°C (1292 or 1382°F). It was also observed that, to obtain useful hardening, the free titanium content must be greater than 1.5%. The weld metal should, therefore, consist of locally hard and soft regions, corresponding to the local concentration of titanium. Although the solidification structure is too fine to isolate dendritic or interdendritic regions for microhardness testing, preferential deformation between these regions has been observed.

Localized Deformation

Localized deformation in the weldment and within the weld solidification structure is observed by the presence of slip steps. As-polished weldment samples plastically deformed in compression leave slip step traces on the specimen surfaces observable under polarized light in the optical microscope.

The welded and aged specimen shown in Fig. 8 exhibits two levels of localized deformation:

1. The weld metal has been strained much more than the HAZ region on the right-hand side of Fig. 8; this follows from tensile and hardness level data showing a significant strength mismatch between base metal and weaker weld metal regions.

2. There is an observable localization of strain within the weld solidification structure itself; this localized strain is the result of an 'easy-path' of deformation following the dendritic regions within the weld.

Preferential deformation of these low titanium concentration regions leave surface topography delineating the cored regions of the solidification structure.

The hardness decrease in the weld metal due to an "easy-path" of deformation should be proportional to the degree of titanium depletion at dendrite cores. Therefore, weldments were given post-weld solution anneal treatments to reduce the severity of segregation in the

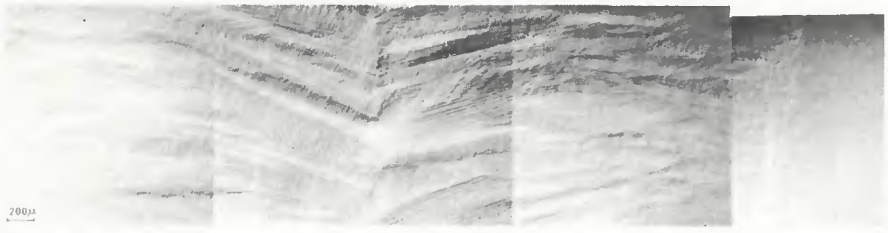

Fig. 8 – Slip localization in aged weldment

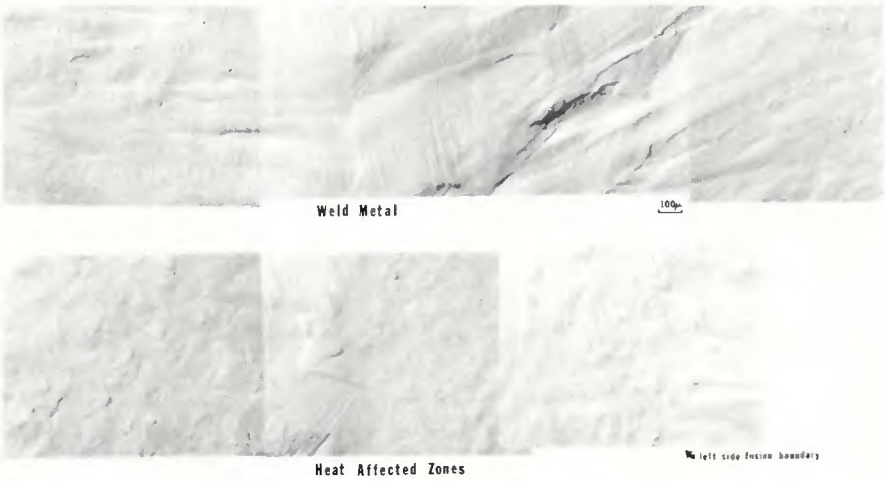

Fig. 9—Slip localization in annealed + aged weldment (top-weld metal; bottom-heat affected zone)

weld metal. An as-polished and deformed weldment specimen given a postweld heat treatment of 10 h at 950°C (1742°F) before aging is shown in Fig. 9. With the exception of a few traces of primary arm dendrite cores, the localized deformation within the solidification structure has disappeared.

It can also be seen that localized strain of the weld metal region has been replaced by much more uniform strain throughout the weldment. This displays the achievement of a close match of strengths in the weldment unobtainable through conventional aging treatments. This is further illustrated by the hardness curves in Fig. 10. The postweld anneals are seen to greatly increase the hardness levels in the weld metal after aging. Weld metal hardness values increase from R_c 22 when aged 24 h at 725°C (1337°F) after welding to above R_c 30 when given the same aging treatment after a solution anneal of 10 h at 950°C (1742°F). This appears to be due to more uniform distributions of titanium resulting in more homogeneous precipitation within the weld metal. Therefore, previous easy-paths of deformation are reduced or effectively removed.

Hardness levels in as-annealed weld specimens are given in Fig. 11. The continued low hardness levels prior to aging display the dependence of the hardness increases on improved weld metal aging responses. Although these as-annealed specimens were observed to contain cellular products in the weld at dendrite interstices in excess of that observed in the as-welded microstructure, the associated decreases in hardness levels upon annealing indicate only a possible detrimental effect by their presence. For toughness considerations, it would most likely be desirable to perform the postweld annealing treatments above the solvus temperature of the cellular products. Hardness decreases in the base metal upon annealing correlate well with observed grain growth, but weld metal grain growth was not apparent.

Although the annealing treatments do not come close to fully homogenizing the weld, a significant reduction in coring is observed in the polished and etched microstructure. The solidification structure of the annealed weldment is very faint relative to the as-welded sample as viewed under identical conditions in the optical microscope. This may be due in part to the removal of low angle boundaries between dendritic and interdendritic regions during annealing. However, clear observations of localized deformation in a recrystallized weld specimen (see Fig. 12), prove these low angle boundaries have little effect on the observance of as-deformed contrast. Localized deformation between dendritic and interdendritic regions are evident even though recrystallization has occurred.

From the large hardness increase in the weld metal after only 1 h at 950°C (1742°F), small increases in titanium concentration must cause significant increases in the level of titanium supersaturation at the dendrite cores. This seems reasonable since Blower and Mayer (Ref. 22) found that titanium concentrations greater than 1.5% were required to obtain useful precipitation behavior in similar alloys. Thus, rapid increases in titanium supersaturation at aging temperatures are expected in regions of near 1.5% titanium concentration upon annealing.

Grain Size

Another factor limiting the weld metal strength is the large columnar grains formed on solidification. These grains are composed of packets of similarly oriented dendrites. The large disparity between the base metal and columnar weld metal grain size is readily apparent. Microhardness traverses were performed to sample hardness values from the regions of vary-

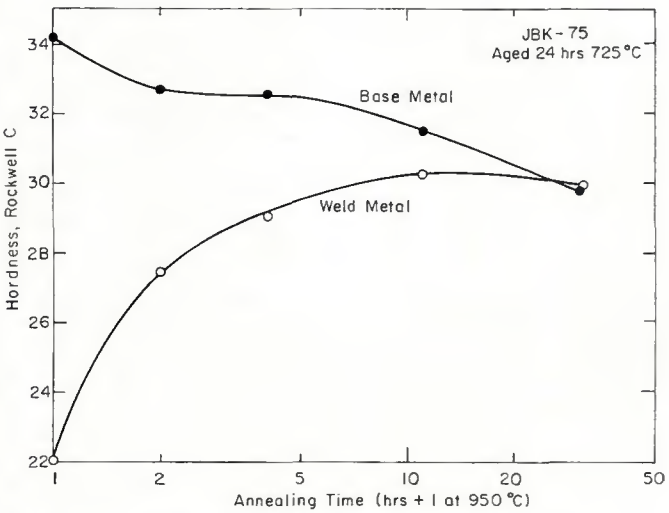

Fig. 10—Hardness curves for JBK-75 after annealing + aging

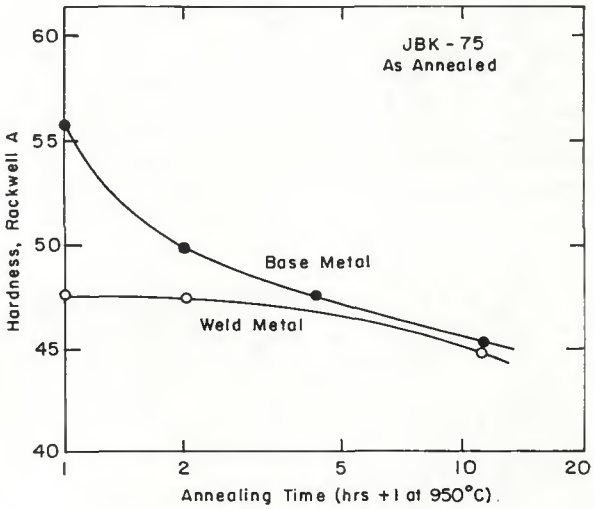

Fig. 11—Hardness curves for as-annealed JBK-75

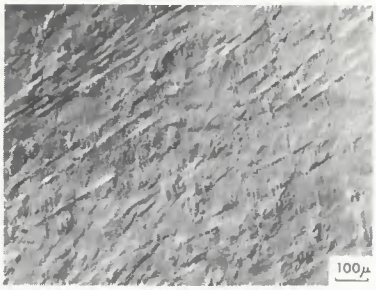

Fig. 12 – Slip localization in recrystallized + aged weldment

ing grain size across the weldment.

Microhardness measurements were made on a Leitz Miniload 2 microhardness tester using a diamond pyramid indentor. Metallographic specimens were prepared from weldments in an identical manner to that used for optical metallography. Indention diameters were measured to the nearest tenth of a micrometer in both directions, averaged and converted into Vickers hardness values. A load of 1000 g (2.2 lb) was used with a 15 s plunge time and 25 s test time taken as standard. Hardness traverses across the weld zones were repeated three times. The average values obtained from each set of three tests corresponding to equivalent regions in the weldment are plotted in Fig. 13.

The results display the significance of grain size on hardness. The finer grained weld metal near the fusion boundaries exhibits increased hardness levels and the enlarged heat-affected zone base metal grains exhibit decreases in hardness. The decrease in base metal hardness after annealing treatments is explained by the observed grain growth.

In order to expose the magnitude of the strength mismatch dependent on grain size differences, the entire weldment was recrystallized. After 25% uniform cold work the weldment was recrystallized/annealed 1 h at 950°C (1742°F). This produced equiaxed weld metal grains matching the grain size of the base metal at ASTM #6. As can be seen in Fig. 14, the resultant grain size is much finer than the original columnar grains still visible through observation of the as-cast dendrite orientations in the polished and etched microstructure. Although the presence of segregation is evident from the cored microstructure, significant hardness increases are expected due to the annealing treatment alone.

Figure 15 compares the base metal and weld metal hardness levels (upon aging) of as-welded, annealed and recrystallized weldment specimens. Figure 15 shows that the matched base and weld metal grain sizes still result in a weaker weld even though weld hardness levels were increased. As-recrystallized (unaged) specimens, on the other hand, possess matching microhardness levels, with the

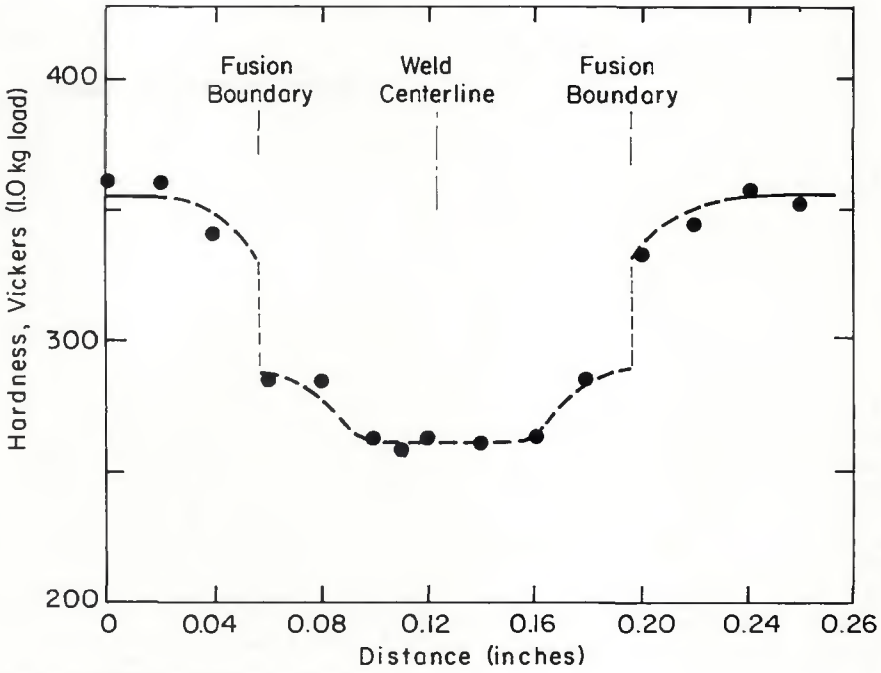

Fig. 13 – Weldment microhardness traverse

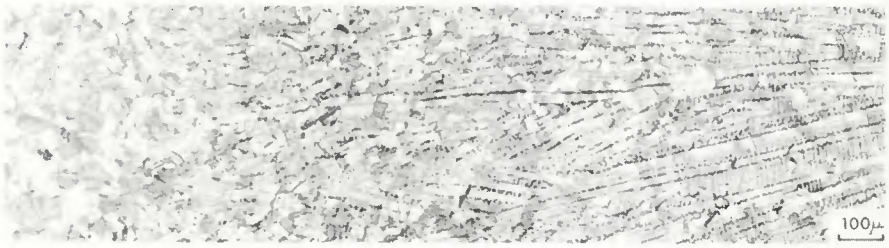

Fig. 14 – Etched microstructure of recrystallized weld

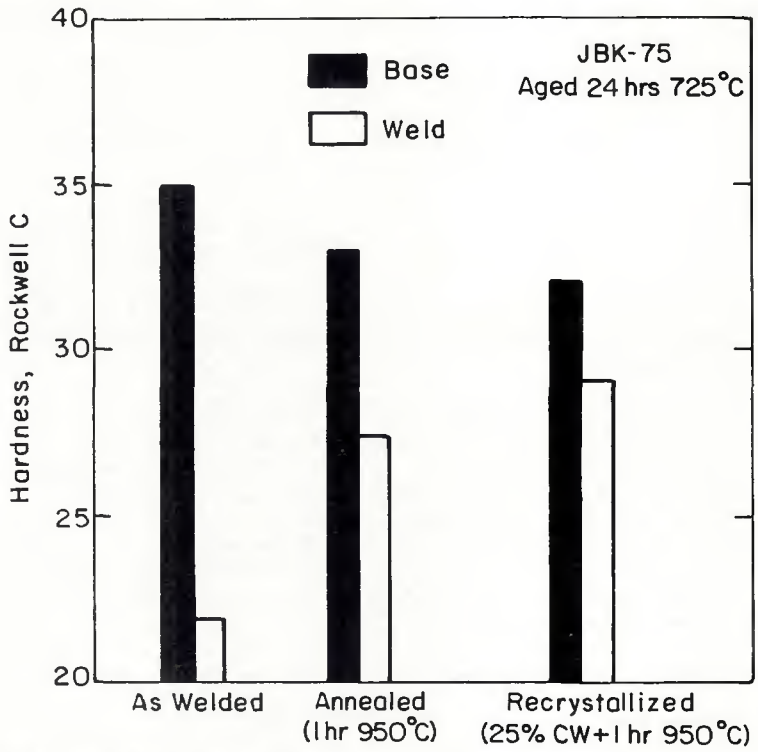

Fig. 15 – Hardness dependence on treatment

weld slightly harder at 156 HV vs. base metal at 152 HV. These results further emphasize the importance of the aging response in determining final strengths in this alloy.

Conclusions

1. A persistent strength mismatch exists in autogenous JBK-75 weldments between base metal and weld metal regions. This can be attributed to both:

(a) Microstructural coarseness from the large columnar weld metal grains.

(b) Chemical segregation of titanium, the major hardening element, to concentrations fluctuating between 1 at-% at dendrite cores and maxima of approximately 5% at dendrite interstices.

2. Chemical segregation in the weld results in the following modification of the aging response consistent with the resistance and hardness curves:

(a) Rapid initial precipitation in titanium enriched regions.

(b) Slower hardness response due to a low density of precipitates in titanium depleted regions.

3. Slip localization occurs in the titanium depleted dendritic regions relative to the enriched interdendritic regions, resulting in an "easy-path" of deformation.

4. Decreased weld microstructural coarseness or columnar grain size results in significant hardness increases.

5. Weldment hardness levels can be matched through post-weld solution annealing treatments prior to aging resulting in:

(a) Increased weld metal hardness.

(b) Uniform deformation within the weld metal.

(c) Decreased base metal hardness due to grain growth.

(d) More uniform strains across weld, HAZ and base metal regions.

6. The magnitude of the weldment strength mismatch decreases at cryogenic temperatures. This may be due to increased resistance to localized deformation by the inhibition of cross slip of widely split dislocations.

7. Weld metal segregation results in the formation of titanium-rich precipitates, believed to be the chi (χ) topographically close-packed phase, not present in the base metal.

Acknowledgments

This research was conducted at the Materials and Molecular Research Division, Lawrence Berkeley Laboratory. The work was supported by the Director, Office of Energy Research, Office of Development and Technology, Magnetic Systems Division and the Office of Basic Energy Sciences, Materials Sciences Division of the U.S. Department of Energy under Contract Number DE-AC03-76SF00098.

References

1. Brooks, J. A., and Krenzer, R. W. 1974. Progress toward a more weldable A-286. *Welding Journal* 53(6):242-s to 245-s.

2. Brooks, J. A. 1974. Effect of alloy modifications on HAZ cracking of A-286 stainless steel. *Welding Journal* 53(11):517-s to 523-s.

3. Garland, J. G. 1974 (April). *Metal Construction and BWJ,* p. 121.

4. Telford, D. G., and Milner, D. R. 1972 (Dec.). *Metal Construction and BWJ,* p. 461.

5. Edvardsson, T. 1979. *Solidification and casting of metals,* p. 424. The Metal Society.

6. Brown, D. C., Crossley, F. A., Rudy, J. F., and Schwartzbart, H. 1962. The effect of electromagnetic stirring and mechanical vibration on arc welds. *Welding Journal* 41(6):241-s to 250-s.

7. Strum, M. J. 1982 (June). M.S. thesis, University of California at Berkeley, LBL-14941.

8. Wilson, F. G., and Pickering, F. B. 1963 *Acta Met.* 16(1):115.

9. Herman, H., Cohen, J. B., and Fine, M. E. 1963. *Acta Met.* 11:43.

10. Mott, N. F. 1937. *J. Inst. Metals* 60:267.

11. Decker, R. F. 1979. *Source book of materials for elevated temperature applications,* ed. E. F. Bradley, p. 275. Metals Park, Ohio: American Society for Metals.

12. Beattie, H. J., Jr., and Hagel, W. C. 1957 (July). *J. Metals,* p. 911.

13. Chang, K. M. 1979 (May). Ph.D. thesis, University of California at Berkeley, LBL-9208.

14. Savage, W. F., and Krantz, B. M. 1971. Microsegregation in autogenous Hastelloy X welds. *Welding Journal* 50(7):292-s to 303-s.

15. Homma, H., Mori, N., and Shinmyo, K. 1979. A mechanism of high temperature cracking in steel weld metals. *Welding Journal* 58(9):277-s to 282-s.

16. Puzak, P. P., Apblett, W. R., and Pellini, W. S. 1956. Hot cracking of stainless steel weldments. *Welding Journal* 35(1):9-s to 17-s.

17. Borland, J. C., and Younger, R. N. 1960 (Jan.). *Metal Construction and BWJ,* p. 22.

18. Sullivan, P., and Donachie, M. J. Jr. 1979. *Source book on materials for elevated temperature applications,* ed. E. F. Bradley, p. 239. Metals Park, Ohio: American Society for Metals.

19. Beattie, H. J. Jr., and Hagel, W. C. 1961 (Feb.). *Trans. of Metall. Soc. of AIME* 221:28.

20. Clark, B. R., and Pickering, F. B. 1967 (Jan.). *J. Iron & Stl. Inst.* 205:70.

21. Owzcarski, W. A., and Sullivan, C. P. 1965. Effect of postweld heat treatment on a superalloy weld deposit. *Welding Journal* 44(6):241-s to 250-s.

22. Blower, R., and Mayer, S. 1963 (Nov.). *J. Iron & Stl. Inst.* 201:933.

23. Headley, T. J., Karnousky, M. N., and Sorenson, W. R. 1982 (March). *Met. Trans. A,* p. 345.